RESEARCH ARTICLE



A global survey of intramolecular isopeptide bonds

Francesco Costa¹ | Ioannis Riziotis¹ | Antonina Andreeva¹ | Delhi Kalwan² | Jennifer de Jong² | Philip Hinchliffe³ | Fabio Parmeggiani^{2,4,5} | Paul R. Race^{2,6} | Steven G. Burston² | Alex Bateman¹ | Rob Barringer²

Correspondence

Rob Barringer, School of Biochemistry, University of Bristol, University Walk, Bristol BS8 1TD, UK.

Email: r.barringer@bristol.ac.uk

Funding information

Biotechnology and Biological Sciences Research Council, Grant/Award Numbers: BB/ T001968/1, BB/T008741/1, BB/W013959/1, BB/X012492/1; EMBL core funds; Engineering and Physical Sciences Research Council, Grant/Award Number: EP/X525674/1

Review Editor: Nir Ben-Tal

Abstract

Many proteins harbor covalent intramolecular bonds that enhance their stability and resistance to thermal, mechanical, and proteolytic insults. Intramolecular isopeptide bonds represent one such covalent interaction, yet their distribution across protein domains and organisms has been largely unexplored. Here, we sought to address this by employing a large-scale prediction of intramolecular isopeptide bonds in the AlphaFold database using the structural template-based software Isopeptor. Our findings reveal an extensive phyletic distribution in bacterial and archaeal surface proteins resembling fibrillar adhesins and pilins. All identified intramolecular isopeptide bonds are found in two structurally distinct folds, CnaA-like or CnaB-like, from a relatively small set of related Pfam families, including 10 novel families that we predict to contain intramolecular isopeptide bonds. One CnaAlike domain of unknown function, DUF11 (renamed here to "CLIPPER") is broadly distributed in cell-surface proteins from Gram-positive bacteria, Gram-negative bacteria, and archaea, and is structurally and biophysically characterized in this work. Using x-ray crystallography, we resolve a CLIP-PER domain from a Gram-negative fibrillar adhesin that contains an intramolecular isopeptide bond and further demonstrate that it imparts thermostability and resistance to proteolysis. Our findings demonstrate the extensive distribution of intramolecular isopeptide bond-containing protein domains in nature and structurally resolve the previously cryptic CLIPPER domain.

KEYWORDS

adhesion, biofilm, fibrillar adhesin, host-pathogen, isopeptide, pilus

1 | INTRODUCTION

The isopeptide bond is a class of covalent amide bond that forms between the amino and carboxamide/carboxyl groups of two side chains of a polypeptide or between a side chain and a terminus. In nature, isopeptide bonds enable either the cross-linking of two points within a single polypeptide chain (intramolecular isopeptide bonds) or between two points of two different polypeptide chains (intermolecular isopeptide bonds). Enzyme-catalyzed

intermolecular isopeptide bonds play a role in many biological processes (Kang & Baker, 2011), including protein ubiquitination, where the target protein is covalently tethered to the ubiquitin protein (Hershko & Ciechanover, 1998); the coagulation pathway, where Factor XIII catalyzes crosslinking of fibrin (Muszbek et al., 1996); and in cell-wall anchored surface proteins of Gram-positive bacteria, whereby pilins are crosslinked to the pentaglycine peptidoglycan bridge at the microbial cell surface (Hendrickx et al., 2011).

This is an open access article under the terms of the Creative Commons Attribution License, which permits use, distribution and reproduction in any medium, provided the original work is properly cited.

© 2025 The Author(s). Protein Science published by Wiley Periodicals LLC on behalf of The Protein Society.

¹European Molecular Biology Laboratory, European Bioinformatics Institute (EMBL-EBI), Hinxton, UK

²School of Biochemistry, University of Bristol, Bristol, UK

³School of Cellular and Molecular Medicine, University of Bristol, Bristol, UK

⁴School of Chemistry, University of Bristol, Bristol, UK

⁵School of Pharmacy and Pharmaceutical Sciences, Cardiff University, Cardiff, UK

⁶School of Natural and Environmental Sciences, Devonshire Building, Newcastle University, Newcastle upon Tyne, UK

Notably, some intermolecular isopeptide bonds form through an autocatalytic mechanism, such as between capsid subunits of various bacteriophages (Helgstrand et al., 2003; Podgorski et al., 2023), where the isopeptide bonds form within a hydrophobic pocket between lysine and asparagine side chains, and are catalyzed by a nearby glutamate side chain (Tso et al., 2017).

Over the past two decades, a second subclass of autocatalytic isopeptide bond has been investigated: the intramolecular isopeptide bond. The first intramolecular isopeptide bond to be structurally resolved was by Kang et al. (2007), housed within the hydrophobic core of a β-sandwich domain of the bacterial pilin Spy0128. This isopeptide bond was formed between the lysine and asparagine (Lys-Asn) side chains of adjacent β-strands, catalyzed by a proximal glutamate side chain (Kang et al., 2007). Subsequently, several other intramolecular isopeptide bond domains (IPDs) have been identified, invariably formed between side chains within the core of β-sandwich folds. These folds can be grouped into two distinct structural families sharing a Greek-key motif: CnaA-like domains (an Ig-like fold that typically forms Lys-Asn cross-links catalyzed by aspartate) and CnaB-like (a transthyretin-like fold that typically forms Lys-Asn or Lys-Asp cross-links catalyzed by a glutamate; Kang & Baker, 2009; Kang & Baker, 2012). In CnaA-like domains, intramolecular isopeptide bond-forming residues are located on opposing β-sheets between the first and penultimate β-strands, while in CnaB-like domains they are positioned on the same β-sheet, between adjacent first and last β-strands. Interestingly, both folds are tolerant of domain insertions within loop regions, usually of intramolecular isopeptide or adhesion domains (Izoré et al., 2010; Pointon et al., 2010; Spraggon et al., 2010; Figure 1).

Functionally, intramolecular isopeptide bonds are thought to enable resistance to various stresses at the cell surface. In 2007, Kang et al. demonstrated that intramolecular isopeptide bonds bestow increased proteolytic resistance and thermostability to the CnaB-like domains of Spy0128, which later proved characteristic of CnaA-like and CnaB-like domains more broadly (Chaurasia et al., 2016; El Mortaji et al., 2012; Hagan et al., 2010; Heidler et al., 2021; Hendrickx et al., 2012; Kang et al., 2007; Kang & Baker, 2009; Kang & Baker, 2011; Zähner et al., 2011). Further work revealed that the intramolecular isopeptide bonds of CnaB-like domains in Spy0128 enable resistance to mechanical unfolding, with these polypeptides proving inextensible under atomic force microscopy (AFM)induced tension (Alegre-Cebollada et al., 2010). In contrast, CnaA-like folds were found to unfold partially under tension, leading to the molecular "shock absorber" hypothesis whereby CnaA-like domains enable adherence under shear forces by dissipating mechanical perturbations (Echelman et al., 2016).

To date, intramolecular isopeptide bonds have primarily been identified in adhesive pili and fibrillar adhesins of Gram-positive bacteria, leading some to question whether they may also be found in Gramnegative bacteria, archaea, eukaryotes, or viruses (Schwarz-Linek & Banfield, 2014). This open question was partially answered in 2021, when an intramolecular isopeptide bond was identified in a pilin of a Gramnegative bacterium (Heidler et al., 2021). Despite this finding, the prevalence and phyletic distribution of intramolecular IPDs in nature have not been systematically probed, and the proteins harboring these domains have not been systematically characterized.

Here, we present the first large-scale prediction of naturally occurring intramolecular isopeptide bonds in the AlphaFold Database, providing insights into their distribution across organisms and protein domains. Using x-ray crystallography, we subsequently resolve an intramolecular isopeptide bond in DUF11, a domain of unknown function found in fibrillar adhesins of Grampositive bacteria, Gram-negative bacteria, and archaea, and confirm that the isopeptide bond imparts significant thermostability and proteolytic resistance. Our work reveals that intramolecular isopeptide bonds frequently appear in stalks of bacterial and archaeal fibrillar adhesins and likely facilitate adherence under various stressful conditions.

2 | RESULTS

2.1 | Characteristics of intramolecular isopeptide bonds

Previous experimental and computational studies revealed that hydrophobic environments likely facilitate intramolecular isopeptide bond formation (Hagan et al., 2010; Hu et al., 2011). However, a comprehensive analysis of the environment of intramolecular isopeptide bonds has not yet been undertaken. Consequently, we first quantified the solvent accessibility of intramolecular isopeptide bonds within protein structures deposited in the PDB and characterized the physicochemical properties of the environment surrounding the bond.

Using a PDB dataset of all known intramolecular isopeptide structures collated in prior work (Costa et al., 2025), we found that the relative solvent accessible surface area (rASA) of most intramolecular isopeptide bonds was <0.05, confirming the buried nature of isopeptide bonds within hydrophobic cores (Kang et al., 2007) (Figure 2a). When assessing *cis/trans* conformations of intramolecular isopeptide bonds, we found that no Lys-Asp bonds are present in the *cis* conformation, while Lys-Asn bonds are equally found in either *cis* (50%) or *trans* (48%) conformations (with 2% found in intermediate conformations). This builds on

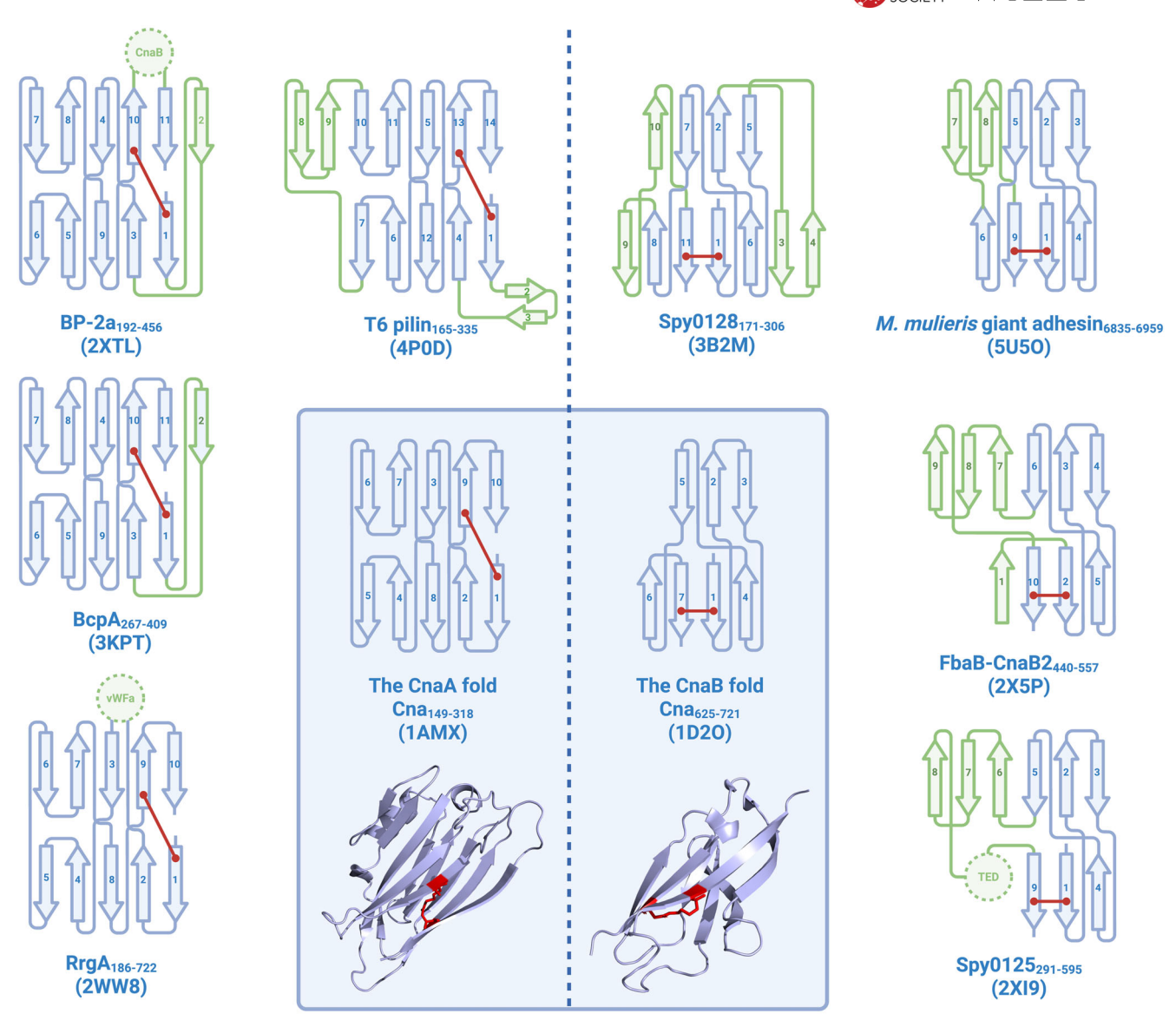


FIGURE 1 β-strand arrangement in CnaA and CnaB folds. Isopeptide bonds are indicated by red lines, along with cartoon depictions of the folds. Alternative CnaA/CnaB topologies are depicted in the periphery. Differences relative to archetypal CnaA/CnaB folds are highlighted in green. Domain inserts are depicted as dotted circles and labeled as follows: CnaB, CnaB-like fold; vWFa, von Willebrand factor type A domain; TED, thioester domain.

our previous observation that 67% of CnaB-like domains favor the *cis* conformation while 73% of CnaA-like domains favor the *trans* conformation (Costa et al., 2025).

To characterize the local environment, we mapped residues within 6 Å of intramolecular isopeptide bonds (Figure S1A). We observed that the surrounding amino acid distributions are similar between CnaA and CnaB-like folds, largely consisting of hydrophobic amino acids and aromatic residues (a feature which has only been qualitatively observed to date, Kang et al., 2007; Kang & Baker, 2011). We noted that the N ζ atom of the isopeptide bond is often located \leq 5 Å above the plane of an aromatic sidechain, with the isopeptide bond N ζ atom $\pm 50^{\circ}$ from the normal of the aromatic ring plane.

This arrangement resembles "above ring" aminoaromatic interactions (Figure 2b,d; Singh Thornton, 1990; Mitchell et al., 1994). We describe aromatic side chains positioned in such a way as "aromatic caps," which appear more prevalent in CnaA-like domains (Figure 2c) but are notably absent in folds harboring insertions of large domains between isopeptide bond-contributing residues (e.g., in the CnaA-like domain of the RrgA pilin and the CnaB-like domain of the Spy0125 pilin; Izoré et al., 2010; Pointon et al., 2010). Aromatic caps are more prevalent in cis Lys-Asn intramolecular isopeptide bonds (94% vs. 24% prevalence in *cis/trans* conformations, respectively), and are absent in all PDB structures containing Lys-Asp bonds. Further analysis found that a consistent

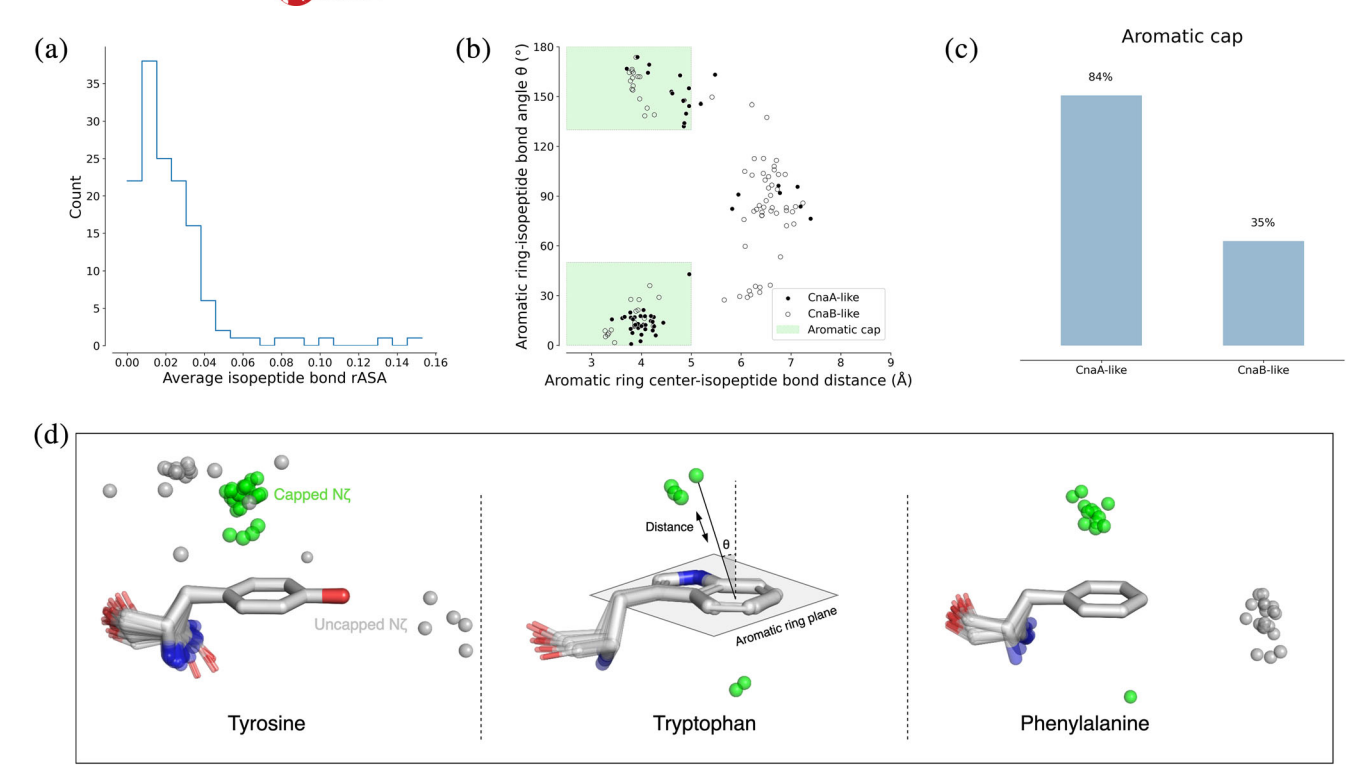


FIGURE 2 (a) Relative accessible solvent area (rASA) averaged across the three isopeptide bond residues. (b) Scatter plot displaying distance and angles between the intramolecular isopeptide bond and aromatic ring plane (distance calculated between the lysine Nζ atom and the centroid of the aromatic ring, angle calculated between the lysine Nζ atom-centroid vector and the normal of the aromatic ring plane). (c) Percentage of intramolecular isopeptide bonds with an aromatic cap, defined as an isopeptide bond within 5 Å of the aromatic ring plane, at an angle <50° or >130° from the normal of the aromatic ring plane (see panel b). Only one PDB entry was assessed per sequence-identical domain. (d) Positioning of Nζ isopeptide bond atoms around their proximal aromatic ring. "Capped Nζ" refers to isopeptide bonds demonstrating an aromatic cap relationship with a proximal aromatic ring. Panels (a), (b), and (d) include redundant proteins.

portion of aromatic caps engage in stacking interactions with proximal isopeptide bonds, while H-bond interactions are rare (again reminiscent of aminoaromatic interactions; Mitchell et al., 1994; Figure S1B). Our analyses also frequently revealed the presence of electron density consistent with a water or ammonia molecule within 5 Å of the intramolecular isopeptide bond oxygen in 54% of CnaB-like and 59% of CnaAlike domains (Table S1), usually buried in the domain core.

2.2 | Large-scale prediction of intramolecular isopeptide bonds in the AlphaFold Database

We next employed a structure-guided search method to identify putative intramolecular isopeptide bonds within predicted structures in the AlphaFold Database (AFDB; Varadi et al., 2024) using the isopeptide-scanning software Isopeptor, which identifies isopeptide bonds in structural models using a template-based matching approach and assigns probability scores to each hit (Costa et al., 2025). We initially tested Isopeptor's ability to detect intramolecular isopeptide bonds in

AlphaFold2 (AF2) models of PDB-deposited intramolecular isopeptide bond structures to confirm that AF2 reliably approximates the positions of isopeptide bond residues. Isopeptor identified intramolecular isopeptide bonds in 94% of AF2 models using a probability threshold of 0.65 (comparable to the recall in PDB structures; Costa et al., 2025), confirming that AF2 places intramolecular isopeptide bond residues in positions consistent with those found in PDB depositions (Figure S2).

Applying Isopeptor to the AFDB using a probability threshold of 0.65, we identified 69,718 intramolecular isopeptide bonds within 33,049 (0.015%) of the 214,683,839 models, all of which were located within βsandwich folds. Since the AFDB does not contain predictions of viral proteins, a scan was also performed against the Big Fantastic Virus Database (BFVD) to determine whether intramolecular isopeptide bonds could be detected in viral proteins (Kim et al., 2025). No hits were returned from the BFVD (data not shown). To characterize the identified intramolecular IPDs into distinct families, we mapped the AFDB Isopeptor hits to Pfam protein domains. The identified domains fell into 26 Pfam families, 12 of which had been structurally characterized with an intramolecular isopeptide bond (Figures 3a and S3, Tables 1 and S2). Multiple hits

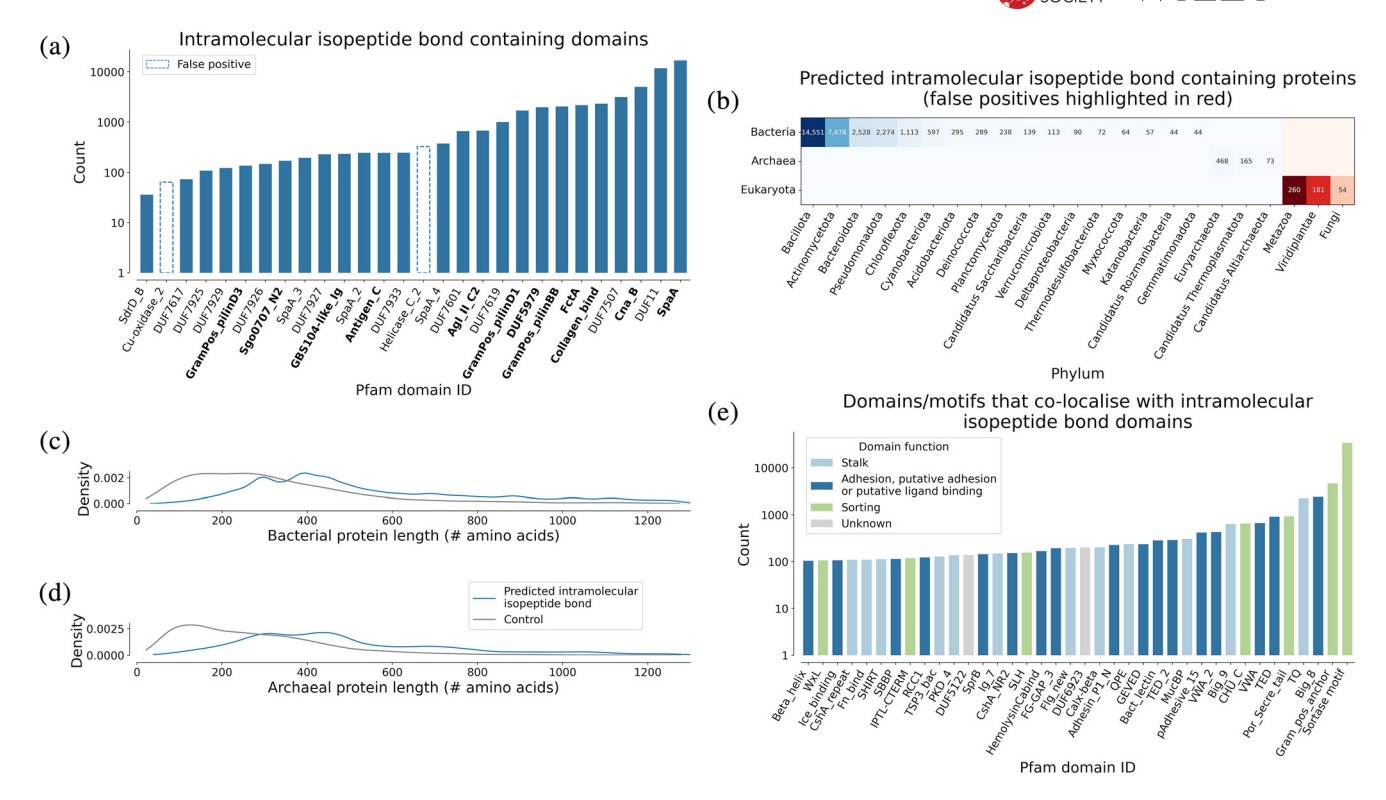


FIGURE 3 (a) Pfam domains predicted by Isopeptor to contain intramolecular isopeptide bonds in the AFDB (probability >0.65). Domains in bold were structurally characterized with an intramolecular isopeptide bond prior to this work. (b) Life domain and phylum distribution of intramolecular isopeptide bond-containing proteins detected with Isopeptor in the AFDB (probability >0.65, phyla with <40 sequences are not shown). Eukaryotic proteins are likely false positives or are from incorrectly annotated organisms. (c, d) Sequence length distribution of bacterial and archaeal intramolecular isopeptide bond proteins detected by Isopeptor in the AFDB. Length distributions are compared with a set of 10,000 randomly selected AFDB proteins from each life domain. Note that the AFDB has an upper sequence length limit of 1280 amino acids. (e) Pfam domains co-occurring with intramolecular IPDs identified by Isopeptor in AFDB proteins. Families were counted once per protein. Domains detected <100 times are not shown (full data are available in Figure S6), nor are domains from polypeptides annotated as eukaryotic.

matched four pre-existing families, two that had been annotated as probable intramolecular IPDs (DUF11 and SpaA_3), and two that had not (SdrD_B and SpaA_2). Many hits did not belong to existing Pfam families and were, therefore, used as seeds to create 10 new Pfam families. All 26 families can be grouped into three superfamilies according to the Pfam classification: the Adhesin (CL0204), Transthyretin (CL0287), and E-set (CL0159) clans.

With an updated collection of intramolecular IPD families, we then surveyed their phyletic distribution in the AFDB. This revealed that intramolecular IPDs are predominantly found in bacterial entries, but we also identified hits within archaea and (Figure 3b). While most intramolecular isopeptide domains are found within the Gram-positive Bacillota and Actinomycetota phyla, a significant number are found within the Gram-negative Bacteroidota and Pseudomonadota phyla. Two previously uncharacterized DUFs were identified in Gram-positive bacteria, Gramnegative bacteria, and archaea: DUF11 and DUF7507, with DUF11 being by far the most broadly distributed (Figure S4). While hits were identified in eukaryotes, manual inspection revealed them to be likely false

positives as the residues were solvent-exposed, not conserved across families, and lacked homologous proteins in related eukaryotes, suggesting that these sequences may have originated from microbial contamination during sequencing projects.

We noted that the proteins identified by Isopeptor are typically longer than other proteins and often harbor tandemly repeating intramolecular isopeptide domains (Figures 3c,d and S5). These domains often co-occur with adhesive domains, particularly Big_8 (a putative adhesion domain related to the collagen-binding domain of the adhesin CNA; Zong et al., 2005), and also stalk domains such as the threonine-glutamine domain (TQ), which possesses a stabilizing intramolecular ester bond (Kwon et al., 2014). Other common cooccurring domains include Gram-negative sorting/ anchoring domains such as Por secre tail and CHU C, and the Gram-positive LPXTG cell wall anchoring motif (Figures 3e and S6). Taken together, these data suggest that a sizable portion of these intramolecular isopeptide bonds occur in elongated surfaceanchored monomeric proteins that enable adhesion, also known as fibrillar adhesins. Subsequent analysis performed using software for fibrillar adhesin detection

TABLE 1 Pfam domains confirmed by structural characterization (bold) or predicted (plain) to harbor intramolecular isopeptide bonds.

Pfam to Pfam to Pfam cacession code Pfam cacession code Pfam to Pfam cacession code Pfam to Pfam cacession code Pf		, , , , , , , , , , , , , , , , , , ,		`	<i>,</i> ,	\(\(\)\)	' '
PF1998 CnaA-like	•	(accession code)- isopeptide bond	accession		domain start-	domain	isopeptide bond residues (first bond residue, catalytic residue, second bond
GPED0623	v – –		5DZ9	Α		554–723	Lys 556, Asp 606, Asn 703
CPF10569 328 436-446 Collagen_bind (PF03737) 7LGR A 173- 173-317 Lys 177, Asp 210, Asn 291 (PF105737) 306 307 308 309	_		4HSS	Α		184–324	Lys 187, Asp 224, Asn 299
Antigen_C			2X9Z	Α			Lys 193, Asp 241, Asn 318
PF16354	_		7LGR	Α		173–317	Lys 177, Asp 210, Asn 291
PEZ5548 DUF7929			3OPU	Α		1330–1489	Lys 1334, Asp 1383, Asn 1469
(PF25551) DUF7926 (PF25546) DUF7926 (PF25546) DUF7927 (PF19407) (PF19408) PECA (PF1802) TW7I A 48			A0A179B332	-		190–349	Lys 193, Asp 241, Asn 334
CF25546			A0A090G7K7	-	81–255	74–257	Lys 86, Asp 129, Asn 213
(PF19407)			Q8YS00	-		260–508	Lys 264, Asp 326, Asn 415
GramPos_pilinD3 (PF16570) FotA (PF12892) GramPos_pilinD1 (PF16555) Cra_B (PF05738) DuF7676 GramPos_pilinD3 (PF16555) Cra_B (PF05738) DuF7676 GramPos_pilinD1 (PF16555) Cra_B (PF05738) DuF7676 GramPos_pilinD1 (PF16555) Cra_B (PF05738) DuF7676 GramPos_pilinD1 (PF16555) Days		•	4BUG	Α		603–718	Lys 610, Glu 680, Asn 715
(PF16570)	SpaA (PF17802)		2XID	Α			Lys 297, Glu 347, Asp 595
GramPos_pilinD1 (PF16555) Cna_B (PF05738) 1D2O A 627— 625—721 Lys 633, Glu 694, Asn 717 T16 SpaA_2 (PF19403) SpaA_3 A0A086ZQG5 - 489— (PF20674) SpaA_4 A0A4R4IAB0 - 700— (PF24514) SdrD_B A0A7C3F8X4 - 157— (PF1210) DUF7601 B8QYD3 - 184— (PF24547) GBS104-like_lg (PF24547) CDBS104-like_lg (PF24589) DUF7619 (PF24346) DUF7619 (PF24346) DUF7617 A0A62BFG97 - 120— DUF7617 (PF24593) DUF7617 A0A495X870 - 676— G78— G78— G78— G78— G78— G78— G78— G78			2X9Z	Α		344–433	Lys 349, Glu 405, Asn 428
(PF16556) Cna_B (PF05738) 1D2O A 627- 625-721 Lys 633, Glu 694, Asn 717 SpaA_2 (PF19403) SpaA_3 (PF20674) SpaA_4 (PF24514) SqrD_B (PF17210) DUF7601 (PF24547) GBS104-like_lg (PF24547) DUF11 (PF01345) DUF7607 DUF7507 A0A2I2KYV6 A0A2I2KYV6 A0A2I2KYV6 A0A6G8FG97 BC293- 489-629 A89-629 A89-629 A89-629 A89-629 A89-629 Lys 497, Glu 571, Asn 627 A89-629, Lys 704, Glu 766, Asn 814 A89-629 A98-629 Lys 497, Glu 571, Asn 627 A89-629 A98-629 Lys 704, Glu 766, Asn 814 A89-629 Lys 159, Glu 263, Asn 248 Asn 248 B14 B153-250 Lys 159, Glu 218, Asn 248 B14 B153-250 Lys 159, Glu 218, Asn 248 B154 B153-250 Lys 190, Glu 263, Asn 305 B12 B17-211, Lys 188, Asp 597, Asn 692 B17-211, Lys 188,	FctA (PF12892)		7W7I	Α	48-216	37–218	Lys 52, Glu 139, Asn 213
SpaA_2			7WOI	Α	48–196	48–196	Lys 57, Glu 158, Asn 195
CPF19403 SpaA_3	Cna_B (PF05738)		1D2O	Α		625–721	Lys 633, Glu 694, Asn 717
PF20674 SpaA_4			A0A086ZQG5	-		489–629	Lys 497, Glu 571, Asn 627
SdrD_B	. –		A0A514BTT6	-		291–412	Lys 298, Glu 353, Asn 409
DUF7601	. –		A0A4R4IAB0	-		696–817	Lys 704, Glu 766, Asn 814
(PF24547) 307 GBS104-like_Ig (PF21426) E-set (CL0159) CnaA-like 3TXA A 587- 137-211, 587-717 Lys 188, Asp 597, Asn 692 DUF11 (PF01345) 9IFR (from this work) A 712- 708-828 Lys 715, Asp 748, Asn 806 DUF7507 (PF24346) A0A2I2KYV6 - 65-169 65-176 Lys 72, Asp 112, Asn 152 DUF7619 (PF24595) L7WFS8 - 653- 655-785 784 Lys 657, Asp 695, Asn 764 DUF7927 (PF25549) A0A6G8FG97 - 120- 119-242 Lys 125, Asp 161, Asn 225 (PF25549) DUF7617 (PF24593) A0A495X870 - 676- 678-807 804 Lys 684, Asp 740, Asn 778 (PF24593) DUF7933 A0A023BX92 - 968- 968- 1096 Lys 973, Asp 1008, Asn 1068			A0A7C3F8X4	-		153–250	Lys 159, Glu 218, Asn 248
(PF21426) CnaA-like 717 587–717 DUF11 (PF01345) 9IFR (from this work) A 712— 708–828 Lys 715, Asp 748, Asn 806 DUF7507 (PF24346) A0A2I2KYV6 - 65–169 65–176 Lys 72, Asp 112, Asn 152 (PF24346) DUF7619 (PF24595) L7WFS8 - 653— 655–785 Lys 657, Asp 695, Asn 764 (PF24595) DUF7927 (PF25549) A0A6G8FG97 - 120— 119–242 Lys 125, Asp 161, Asn 225 (PF25549) DUF7617 (PF24593) A0A495X870 - 676— 678–807 Lys 684, Asp 740, Asn 778 (PF24593) DUF7933 A0A023BX92 - 968— 968—1096 Lys 973, Asp 1008, Asn 1068			B8QYD3	-		184–308	Lys 190, Glu 263, Asn 305
this work) 812 DUF7507 (PF24346) DUF7619 (PF24595) DUF7927 (PF25549) DUF7617 (PF24593) DUF7933 A0A023BX92 - 968-1096 Lys 72, Asp 112, Asn 152 Lys 72, Asp 112, Asn 152 Lys 657, Asp 695, Asn 764 Lys 657, Asp 695, Asn 764 Lys 125, Asp 161, Asn 225 Lys 684, Asp 740, Asn 778 Lys 684, Asp 740, Asn 778 Lys 684, Asp 740, Asn 778 Lys 973, Asp 1008, Asn 1068	_ •	,	3TXA	Α			Lys 188, Asp 597, Asn 692
(PF24346) L7WFS8 - 653- 785 784 Lys 657, Asp 695, Asn 764 (PF24595) A0A6G8FG97 - 120- 119-242 193 Lys 125, Asp 161, Asn 225 (PF25549) 250 Lys 684, Asp 740, Asn 778 (PF24593) A0A023BX92 - 968- 1096 196 Lys 973, Asp 1008, Asn 1068	DUF11 (PF01345)		,	Α		708–828	Lys 715, Asp 748, Asn 806
(PF24595) 784 DUF7927 (PF25549) A0A6G8FG97 - 120- 250 119-242 Lys 125, Asp 161, Asn 225 DUF7617 (PF24593) A0A495X870 - 676- 678-807 B04 Lys 684, Asp 740, Asn 778 DUF7933 A0A023BX92 - 968- 968-1096 Lys 973, Asp 1008, Asn 1068			A0A2I2KYV6	-	65–169	65–176	Lys 72, Asp 112, Asn 152
(PF25549) 250 DUF7617 A0A495X870 - 676- 678-807 Lys 684, Asp 740, Asn 778 (PF24593) Lys 684, Asp 740, Asn 778 804 DUF7933 A0A023BX92 - 968- 968-1096 Lys 973, Asp 1008, Asn 1068			L7WFS8	-		655–785	Lys 657, Asp 695, Asn 764
(PF24593) 804 DUF7933 A0A023BX92 - 968- 968-1096 Lys 973, Asp 1008, Asn 1068			A0A6G8FG97	-		119–242	Lys 125, Asp 161, Asn 225
			A0A495X870	-		678–807	Lys 684, Asp 740, Asn 778
			A0A023BX92	-		968–1096	Lys 973, Asp 1008, Asn 1068

(Monzon & Bateman, 2022) revealed that 14% of intramolecular isopeptide bond-containing proteins identified in the AFDB by Isopeptor are likely to be fibrillar adhesins. Indeed, inspection of the Isopeptor hits identified several putative fibrillar adhesins in Gram-positive bacteria, Gram-negative bacteria, and archaea, covering pathogens, opportunistic pathogens, and commensal microbes (Figure S7, Table S3).

Fibrillar adhesins typically present as domainshuffled polypeptides with unique functionalities, dictated by the specific domain arrangements within the protein structure (Barringer et al., 2023; Monzon et al., 2021). Thus, we next characterized domains that co-occur with intramolecular IPDs in AFDB polypeptides. Our analyses found a diverse set of co-occurring domains which can be broadly divided into three functional categories: adhesion, stalk-forming, and sorting domains (Figure 3e), mainly from bacteria (Figure S6). While intramolecular IPDs (primarily DUF11) were identified in archaeal AFDB proteins, co-occurring domains were rarely detected, indicating that either these structures contain only DUF11 repeats or that co-occurring domains do not resemble the current collection of known Pfam domain families. When other domains are present in archaea, they commonly include the Chlam PMP domain (Pfam ID PF02415), which is also found in Chlamydia surface proteins, and PKD 4 domains (Pfam ID PF18911), which have also been detected in bacterial surface proteins. We noted that proteins of the archaeal kingdom Methanobacteriati frequently employ C-terminal protein sorting motifs (e.g., Pfam IDs PF18204, PF26597, and PF26596), which enable covalent attachment of the C-terminus to the cell surface by archaeosortases A (ArtA), B (ArtB), and C (ArtC), likely via attachment of lipid moieties (Haft et al., 2012).

2.3 | DUF11 is an intramolecular IPD that is widely distributed in fibrillar adhesins of bacteria and archaea

The DUF11 domain family was initially deposited in the Pfam database in 1998 (Pfam ID: PF01345) and was rebuilt in 2018 to better represent several immunoglobulin-like domains, some of which were predicted to engage in intramolecular isopeptide bond formation. AF2 predicts that DUF11 domains fold into an Ig-like β -sandwich structure containing a Greekkey motif and consisting of seven to nine β -strands. While DUF11 belongs to the E-set Ig-like fold clan (CL0159), it shares some topological similarity to domains of the bacterial adhesin clan (CL0204), which both represent CnaA-like domains (Table 1). Typically, DUF11 domains are found in one or multiple copies, often tandemly repeated in the middle of long proteins harboring a signal peptide, adhesion

domains, and sorting domains, indicating that the domain routinely forms the stalk of fibrillar adhesins (Figure 4). While all DUF11 domains share global sequence similarity and are predicted to exhibit a CnaA-like fold, some DUF11 domains appear to lack intramolecular isopeptide bonds (Table S2). This heterogeneity is evident from the Pfam SEED and FULL alignments, in which the positions of the residues predicted to form isopeptide bonds are not universally conservked.

While most DUF11 domains are found in proteins from Gram-positive and Gram-negative bacteria, some have been identified in multiple cell-surface proteins from archaea. Tandem DUF11 repeats are present in proteins that resemble fibrillar adhesins of the archaean genus Methanothermobacter (Sumikawa et al., 2019) and are present in porins (mostly without isopeptide bond signatures) that are proposed to form part of the archaeal S-layer structure (Doloman et al., 2024). DUF11-containing Methanothermobacter proteins are known to stabilize cell aggregates, and while the role of DUF11 domains in these cell proteins remains cryptic, they are suspected to be important for stabilization of the protein (Sumikawa et al., 2019). It has also been demonstrated that adhesin-like proteins of Methanothermobacter species are frequently acquired as a result of lateral gene transfer from bacteria, some of which contain DUF11 domains (e.g., Msm 1533; Lurie-Weinberger et al., 2012).

DUF11 is closely related to DUF7507, a new Pfam family built from IPDs identified by Isopeptor. DUF7507 domains are more compact than DUF11, typically consisting of seven β-strands (as judged by the AF2 predictions). Both DUF11 and DUF7507 domains are frequently found in tandem within surface polypeptides of bacteria and archaea, often alternating between the two families in tandem. Given the likely propensity of DUF11 and DUF7507 domains to harbor intramolecular isopeptide bonds, we have renamed and refer to them hereafter as CLIPPER and CLIPPER 2 domains (Cross-Linked IsoPeptide Protein in the Extracellular Region). Despite their wide phyletic distribution in a variety of putative host-binding fibrillar adhesins, neither CLIPPER nor CLIPPER 2 has previously been structurally or biophysically characterized. For this reason, we proceeded to determine the structure of a member of the CLIPPER family using x-ray crystallography to confirm the presence of an intramolecular isopeptide bond and undertook biophysical studies to characterize the thermal and proteolytic resilience of this domain.

2.4 | Structural and biophysical characterization of a CLIPPER domain

We chose to structurally and biophysically characterize a CLIPPER domain from a putative fibrillar adhesin

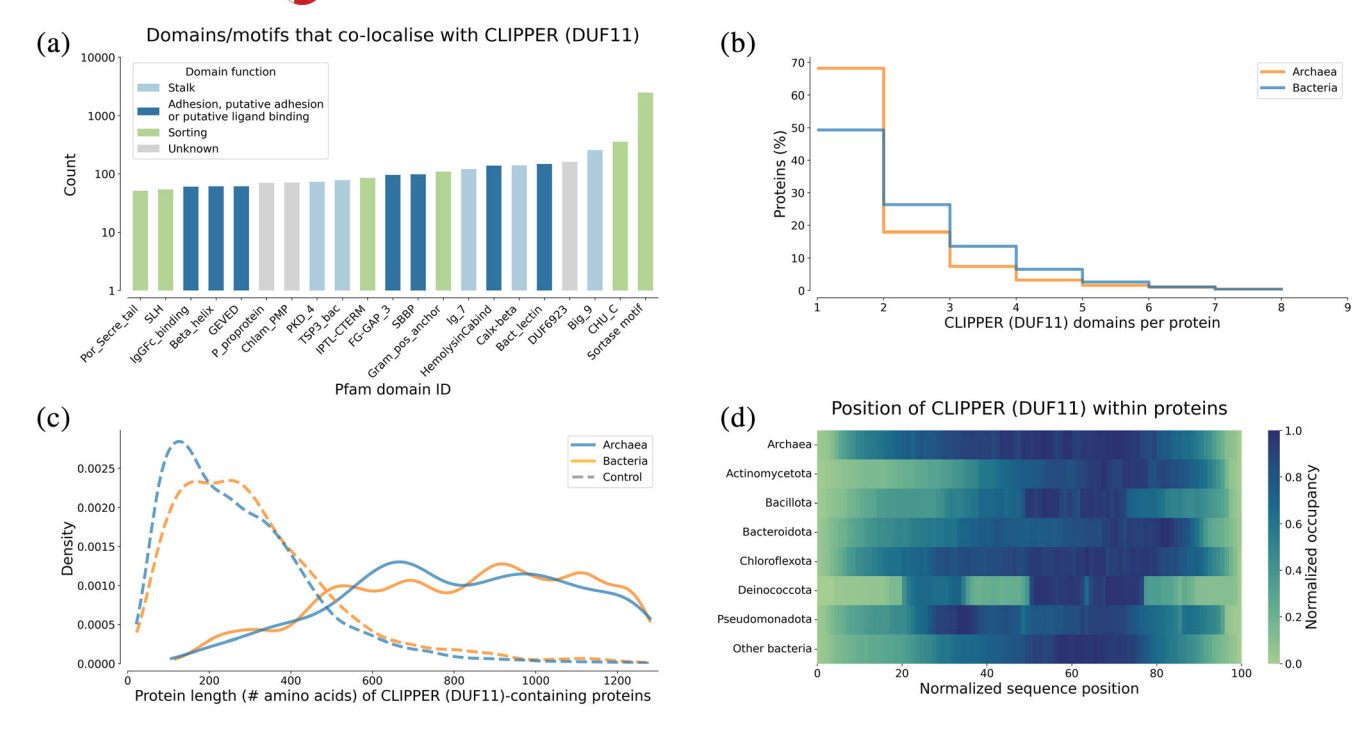


FIGURE 4 (a) Pfam domains co-occurring with CLIPPER IPDs in bacterial and archaeal AFDB proteins (domains detected <50 times are not shown). (b) Histogram showing the number of CLIPPER IPD repeats per AFDB protein. (c) Protein length distribution of AFDB proteins with at least one CLIPPER IPD, compared to control sequences as described in Figure 3. (d) Positioning of CLIPPER IPDs within AFDB polypeptide sequences of archaea and various bacterial phyla.

utilized by a Gram-negative bacterium within a well-characterized, high-quality genome. To this end, we identified a putative fibrillar adhesin 2129 amino acids in length from the genome of *Acinetobacter silvestris* ANC 4999 (Nemec et al., 2022), named B9T28_05395 (Uniprot ID: A0A1Y3CHT7_9GAMM). This fibrillar adhesin appears to be composed of an N-terminal adhesive CshA_NR2-like domain, a CshA_GEVED-like domain, a tandem repeat stalk of either CLIPPER domains or C-terminal cadherin-like domains, and an OmpA-like anchoring domain (Figure 5a). The CLIP-PER repeat between residues 708–828 demonstrated the highest average identity to the other CLIPPER repeats (data not shown) and was subsequently chosen for experimental characterization.

Constructs of wild-type CLIPPER (CLIPPER_{WT}) and a variant lacking the predicted isopeptide-forming lysine (CLIPPER_{K715A}) were expressed, purified (Figure S8), and their His-tag cleaved off prior to crystallization attempts. Following sparse-matrix screening of various crystallization conditions, CLIPPER_{WT} crystals were acquired, with data extending to 1.77 Å resolution (Table 2). The final modeled structure consists of a β -sandwich formed by two antiparallel sheets of four and five β -strands (Figure 5b). The domain presents as a CnaA-like fold (Figure 5c) and exhibits an intramolecular isopeptide bond between Lys-715 and Asn-806, presumably catalyzed by nearby Asp-748 (Figure 5d). The final β -strand (β 9) of the fold exhibits a mid-strand β -

bulge that is caused by a tetrapeptide disulfide motif of Cys-818/Thr-819/Thr-820/Cys-821 (Figure 5e). The observation of a tetrapeptide disulfide bond motif prompted us to investigate the wider disulfide prevalence in intramolecular IPDs. We found that disulfide bonds co-occur alongside isopeptide bonds in 29.7% and 34.9% of CLIPPER and CLIPPER_2 domains respectively at various sites. We also noted that disulfide bonds are prevalent in IPD families SpaA_2, SpaA_3, SpaA_4, and DUF7933 domains (Table S4). They are predominantly found in the Gram-positive Actinomycetota (in 41.3% of intramolecular IPDs), and in Gram-negative Acidobacteriota (79.2%), Pseudomonadota (58.2%), and Chloroflexota (42.7%; Table S5).

We next sought to characterize the stabilizing effects of the intramolecular isopeptide bond on CLIP-PER. Since intramolecular isopeptide bonds usually significant thermotolerance to CnaA-like domains (Heidler et al., 2021), we investigated the thermal stability of CLIPPERWT and the isopeptide-lacking CLIPPER_{K715A} using circular dichroism (CD) by collecting spectra from 5°C to 95°C at 5°C intervals (Figure 6a). CLIPPERWT and CLIPPERK715A demonstrate comparable β-sheet-like spectra, with a negative mean residue ellipticity (MRE) at 218 nm and positive MRE at <200 nm, indicating that both constructs are folded. At higher temperatures, a transition to a disordered state is observed for both constructs, at \sim 80°C CLIPPER_{WT} and ~45°C for CLIPPER_{K715A}

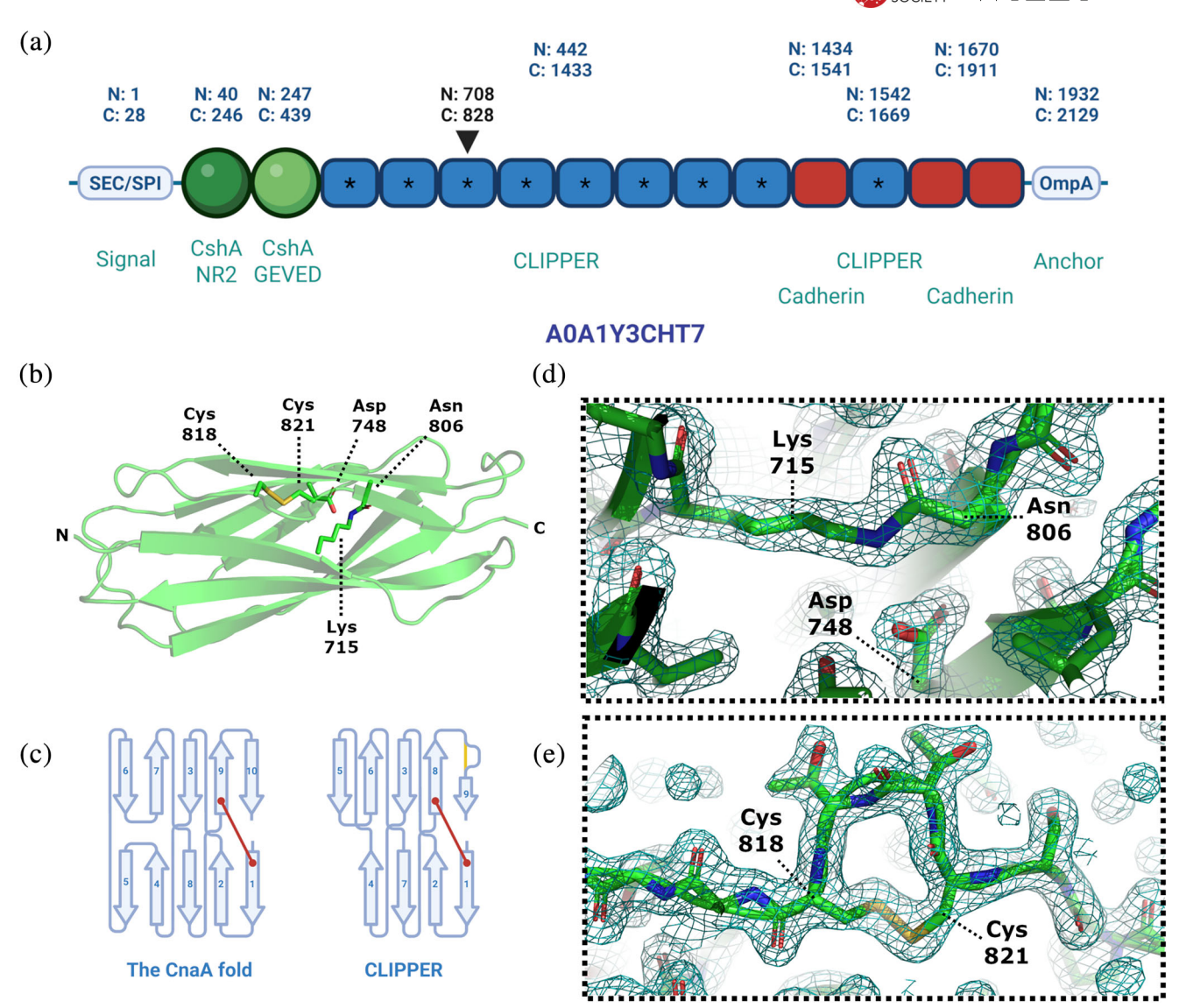


FIGURE 5 (a) Schematic of fibrillar adhesin B9T28_05395 from *Acinetobacter silvestris* ANC 4999, with N- and C-termini of domain regions indicated. The black arrow indicates the CLIPPER domain investigated in this work (residues 708–828). Asterisks indicate CLIPPER domains predicted by Isopeptor to contain intramolecular isopeptide bonds. (b) A PyMOL rendering of the x-ray crystal structure of CLIPPER_{WT}, depicted in cartoon format. Residues involved in intramolecular isopeptide bond and the tetrapeptide disulfide motif formation are shown in stick format, and labeled. (c) Comparative topology diagrams of CLIPPER_{WT} and the classic CnaA fold. Isopeptide bonds are indicated by a red line, and disulfide bonds as a yellow line. (d) A zoomed-in view of the isopeptide bond and putative catalytic aspartate of the CLIPPER_{WT} domain, depicted in stick format. (e) A zoomed-in view of the CTTC disulfide motif. Electron density maps are shown in teal and contoured to 1σ (0.314 e/ų).

(Figure 6c). At high temperatures, the MRE values at 203 nm appear to differ between the polypeptides, reaching a plateau of $\sim\!\!-7500\,\mbox{deg.cm}^2.\mbox{dmol}^{-1}$ in CLIPPER_{WT} and $\sim\!\!-10,\!000\,\mbox{deg cm}^2\,\mbox{dmol}^{-1}$ in CLIPPER_{K715A} (Figure 6a,c), indicating that the intramolecular isopeptide bond may prevent total unfolding of the polypeptide chain.

We then assessed whether the intramolecular isopeptide bond facilitates refolding from thermally denatured states. To this end, the samples were subsequently cooled from 95°C to 5°C, with spectra collected at 5°C intervals (Figure 6b,c). During cooling,

CLIPPER $_{\text{WT}}$ appears to regain a predominantly β -sheet structure, whereas CLIPPER $_{\text{K715A}}$ does not, with MRE between 200 and 205 nm failing to achieve a positive value. When plotting the folded-unfolded-refolded transition at 203 nm, both constructs demonstrate rapid unfolding but gradual refolding (which is incomplete for CLIPPER $_{\text{K715A}}$; Figure 6c). These data indicate that the intramolecular isopeptide bond of CLIPPER bestows significant thermotolerance to the domain and enables efficient refolding of the domain upon cooling.

Finally, we sought to test the proteolytic susceptibility of $CLIPPER_{WT}$ and $CLIPPER_{K715A}$ to determine

TABLE 2 Crystallography data collection and refinement statistics for the CLIPPER domain (residues 708–828 of B9T28_05395).

Crystallography da	ta collection and r	refinement
--------------------	---------------------	------------

Data collection			
Space group	P6 ₃		
Unit cell dimensions (Å): A, B, C	93.859, 93.859, 21.994		
Unit cell angles (°): α, β, γ	90, 90, 120		
Datasets merged	2		
Resolution (Å)	81.28–1.77 (1.80– 1.77)		
CC1/2 (%)	0.993 (0.401)		
R_{pim}	0.161 (3.626)		
Number of unique reflections	11,209 (547)		
Multiplicity	38.7 (29.5)		
Overall signal-to-noise ratio (I/σ)	5.1 (0.4)		
Completeness (%)	99.91 (97.16)		
Refinement			
<i>R</i> work	0.200		
<i>R</i> free	0.209		
No protein atoms used in refinement	876		
No water atoms used in refinement	113		
B factors for protein atoms (Å ₂)	31.89		
B factors for water atoms (Å ₂)	36.29		
RMS deviations—length (Å)	0.015		
RMS deviations—angle (°)	1.544		
Ramachandran-favored residues (%)	97		

Note: Values in parentheses are for the highest resolution shell ($CC_{1/2} > 0.4$ used to decide resolution cut-off).

1

Ramachandran outlying residues

whether the intramolecular isopeptide bond imparts proteolytic resistance (as observed in other intramolecular IPDs; Kang & Baker, 2009). Recombinant CLIP-PER_{WT} and CLIPPER_{K715A} polypeptides were incubated with Proteinase K at 20°C, 30°C, 40°C, and 50°C for 1 h and visualized using sodium dodecyl sulfate polyacrylamide gel electrophoresis (SDS-PAGE). The results revealed that CLIPPER_{WT} is significantly more resistant than CLIPPER_{K715A} to proteolysis when treated with Proteinase K over all temperatures (Figure 6d), indicating that the presence of the isopeptide bond confers significant proteolytic resilience to the fold, in line with the properties of other intramolecular IPDs (Kang & Baker, 2009).

3 | DISCUSSION

To resist the significant mechanical forces at play during adherence to a surface (Busscher & van der Mei, 2006), microbial adhesins are known to employ

various strategies to stabilize the extended protein and resist various stresses. While some strategies employ non-covalent interactions for this purpose (Lipke, 2025; Vance et al., 2020), covalent cross-links have also been postulated to provide significant resilience to adhesins under mechanical stress. Such covalent strategies include intramolecular isopeptide bonds (Alegre-Cebollada et al., 2010; Echelman et al., 2016), intramolecular ester bonds (Lei et al., 2021), and intermolecular thioester bonds, which covalently bind host surfaces and maintain adherence under strong mechanical forces (Alonso-Caballero et al., 2020; Walden et al., 2015).

This work characterized common environmental features surrounding intramolecular isopeptide bonds and surveyed their distribution in nature. Our analyses quantitatively confirm previous observations that these bonds are invariably found within hydrophobic cores, often near aromatic residues (Figure 2; Kang et al., 2007; Kang & Baker, 2009). We found that many intramolecular isopeptide bonds position the lysine Nζ atom in a pose resembling "above ring" aminoaromatic interactions (stacked interactions within 5 Å of the ring centroid and within 50° of the normal of the aromatic plane, Singh & Thornton, 1990; Mitchell et al., 1994). These "aromatic caps" (as referred to herein) are detected in 84% and 35% of CnaA-like and CnaB-like domains respectively, in 94% and 24% of isopeptide bonds in cis/trans conformations, and are notably absent in folds containing Lys-Asp bonds. Their prevalence may suggest that aromatic caps play a functional role in intramolecular IPDs. For example, aromatic caps might function as a recruitment site for isopeptide-forming side chains, creating positions conducive to bond formation during protein folding. Alternatively, the aromatic planes may interact with polar moieties of the isopeptide bond residues in stacked orientations to reduce entropy within the hydrophobic core. Future work investigating the rate of isopeptide bond formation and domain entropy in aromatic vs. non-aromatic folds may clarify whether they play a functional role in isopeptide bond formation and domain stabilization.

In more than half of the surveyed structures, we found electron densities consistent with water or ammonia molecules proximal to isopeptide $\mathrm{Asn}_{\mathrm{O}\delta}$ / $\mathrm{Asp}_{\mathrm{O}\delta}$ atoms. It is not clear whether the presence or absence of such molecules reflects distinct optimizations of the chemical environment. It may be that their frequent occurrence within the domain core represents channels that enable the release of byproducts upon bond formation (as suggested previously, Hagan et al., 2010; Hu et al., 2011). Alternatively, they may play a stabilizing role within the domain interior via key hydrogen-bond interactions.

Intramolecular IPDs appear to group closely within three superfamily clans. Two extant domain families

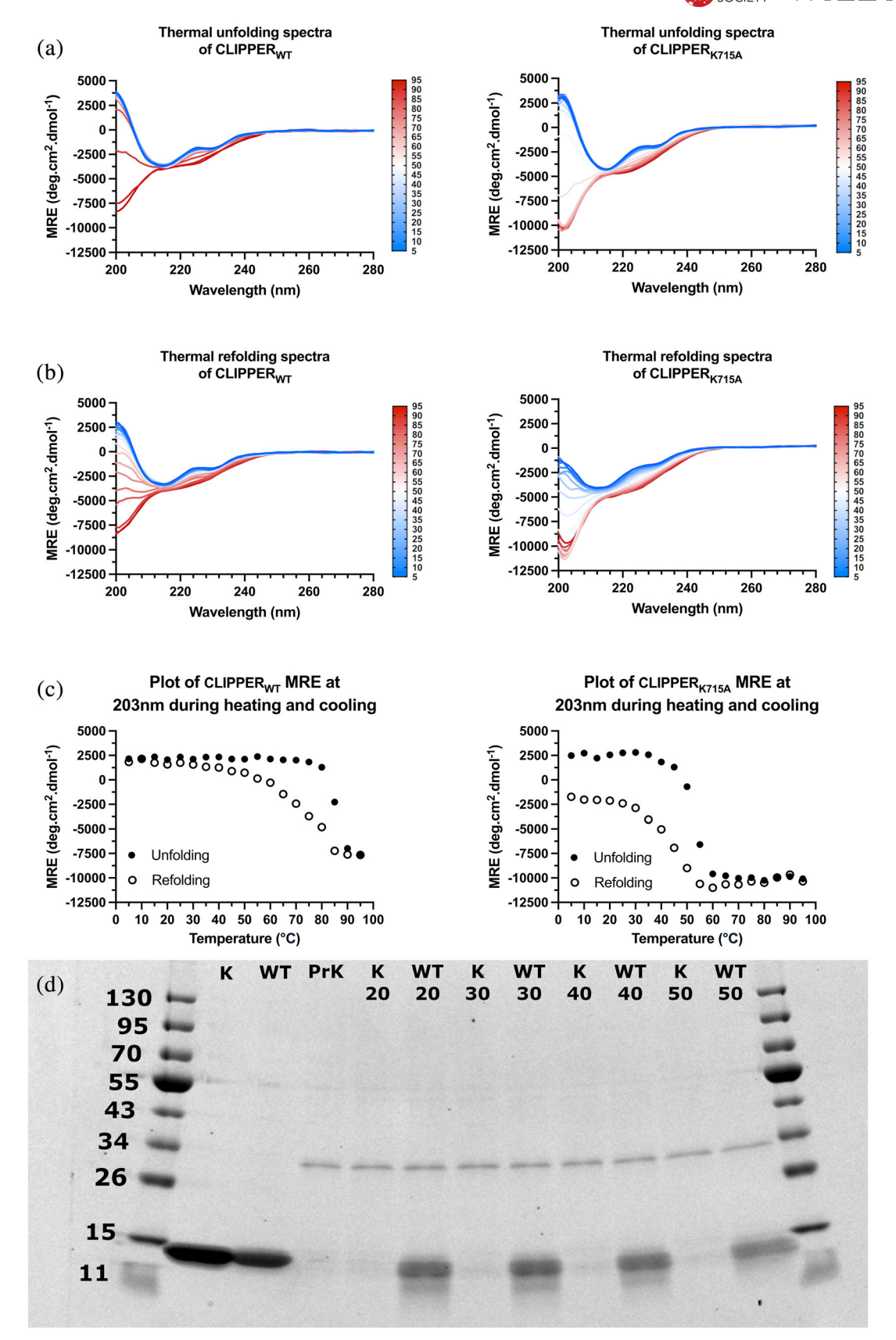


FIGURE 6 (a) CD thermal unfolding spectra of CLIPPER $_{\text{WT}}$ and CLIPPER $_{\text{K715A}}$, increasing from 5°C to 95°C with spectra recorded at 5°C increments. (b) CD thermal refolding spectra of CLIPPER $_{\text{WT}}$ and CLIPPER $_{\text{K715A}}$, decreasing from 95°C to 5°C with spectra recorded at 5°C increments. (c) 203 nm MRE plot of CLIPPER $_{\text{WT}}$ and CLIPPER $_{\text{K715A}}$ during thermal unfolding and refolding. (d) SDS-PAGE analysis of CLIPPER $_{\text{WT}}$ (WT) and CLIPPER $_{\text{K715A}}$ (K) polypeptides after incubation with buffer or Proteinase K (PrK) at the indicated temperatures (in degrees Celsius) for 1 h.

had not been annotated as intramolecular IPD families prior to this work (SdrD-B and SpaA 3), while two (DUF11 and SpaA_3) were annotated as such in the Pfam database but lacked experimental validation. Ten new families were created, expanding the repertoire of known intramolecular isopeptide domain families to 26 (Table 1). Considering that all 26 families are predicted to resemble β-sandwich folds with Greek-key motifs, it is likely that CnaA-like and CnaB-like folds share a common evolutionary origin. While our results have not identified intramolecular isopeptide bonds in non-β-sandwich folds, recent work has introduced an autocatalytic intramolecular isopeptide bond to a βsandwich fold lacking the Greek-key motif, indicating that such bonds can exist in non-CnaA/CnaB-like folds (Srisantitham et al., 2025). Indeed, other work has described a naturally occurring autocatalytic intermolecular isopeptide bond in an α-helical hairpin fold (Remaut, Sleutel & Sogues 2025), indicating that αhelical folds are capable of forming isopeptide bonds. Future studies employing the findings of this work and protein design tools may elucidate whether isopeptide bonds can be engineered into alternative synthetic folds to generate stabilized synthetic domains for novel adhesive and material technologies.

Until now, only one intramolecular IPD has been structurally characterized from an organism that is not a Gram-positive bacterium (Heidler et al., 2021), and their wider phyletic distribution has remained uncertain (Schwarz-Linek & Banfield, 2014). We found that intramolecular isopeptide bonds are prevalent in Grampositive bacteria, but that three families demonstrate wider distribution. DUF11 (renamed CLIPPER) and the closely related domains DUF7507 (renamed CLIP-PER 2) and DUF7619 are frequently found in polypeptides of Gram-negative bacteria, while CLIPPER and CLIPPER 2 also occur in archaeal proteins (Figure S4). We found that tandemly repeating intramolecular IPDs are usually located in elongated cell-surface proteins of host-binding pathogens, opportunistic pathogens, and commensal (Figures 3, S7, and Table S3). Notably, CLIPPER appears to be the most widely distributed domain, often tandemly repeated in the stalks of fibrillar adhesins (Figures 4 and S4). The frequent use of tandemly repeating intramolecular isopeptide bonds in fibrillar adhesins of host-binding bacteria and archaea indicates that they may be important for the efficient colonization of host tissues and may, therefore, present attractive targets for novel antimicrobial therapeutics. Future work may focus on generating novel therapeutics to interfere with isopeptide bond formation and abrogate host colonization by pathogens, following previous work that has demonstrated promising results employing this strategy (Rivas-Pardo et al., 2018).

Given that CLIPPER was found to be the most broadly distributed intramolecular isopeptide domain

from our work, we experimentally characterized an fibrillar exemplary domain from the B9T28 05395 of Acinetobacter silvestris ANC 4999. Our crystal structure reveals that the CnaA-like fold harbors an intramolecular isopeptide bond between Lys-715 and Asn-806, presumably catalyzed by Asp-748 (Figure 5). The isopeptide bond enables significant thermostability and resistance to proteolysis and can refold after thermal denaturation, properties that were abrogated in an isopeptide-lacking variant (Figure 6). This indicates that the isopeptide bond of CLIPPER domains enables significant resilience to stress, which is likely of functional importance when present in the stalks of fibrillar adhesins from Gram-positive bacteria, Gram-negative bacteria, and archaea.

This body of work indicates that intramolecular isopeptide bonds are broadly utilized in nature to stabilize adhesin stalks faced with various stresses. Whether other covalent intramolecular bonds are as widely distributed is not currently known. Further work investigating the distribution of such bonds in the AFDB may probe their phyletic distribution in nature, reveal key features of their chemical environments, and inform design processes aiming to introduce covalent intramolecular bonds into synthetic folds.

4 | MATERIALS AND METHODS

4.1 | Analysis of intramolecular isopeptide bond structural features

Wild-type PDB structures containing an intramolecular isopeptide bond, with x-ray diffraction resolution ≤2.5 Å and unusual residue no properties (e.g., incomplete or missing isopeptide bond triad side chains present on flexible loops), were chosen from the previously collated collection of intramolecular IPDs (Costa et al., 2025). This dataset includes remodeled structures of intramolecular isopeptide bonds, which have been deposited in the PDB with incorrect isopeptide bond geometries. Only one PDB entry was assessed per sequence-identical domain, considering the 20 residues flanking each side of the first and last isopeptide bond signature positions, unless specified otherwise. rASA was calculated using the Biotite package v1.3.0 (Kunzmann & Hamacher, 2018) sasa function with point_number 500 and values normalized using Rost and Sander maximum ASA values (Rost & Sander, 1994). Bonds were classified as cis for pseudo ω angles <60° or trans for angles >120°. "Aromatic caps" were identified as aromatic residues with the centroid of their aromatic ring within 5 Å of the isopeptide bond Lys_{NC} atom, where the angle between the centroid-Lys_{Nr} atom vector was <50° or >130° from the normal of the aromatic ring plane (in the case of tryptophan,

the closest of the two rings was considered). Where no aromatic caps were detected, the closest aromatic within 10 Å of the Lys $_{N\zeta}$ atom was plotted. The analyses were conducted with custom python v3.12.2 scripts with the Biotite, Pandas v2.1.1 (McKinney, 2010), seaborn v0.13.2 (Waskom, 2021), matplotlib v3.8.0 (Hunter, 2007), biopython v1.83 (Cock et al., 2009), and Numpy v1.26.4 (Harris et al., 2020) packages for calculations.

4.2 | AlphaFold2 modeling

AlphaFold2 modeling was performed on A100 GPUs with AlphaFold version 2.3.1 (Jumper et al., 2021) (https://github.com/kalininalab/alphafold_non_docker) and cuda version 11, with active amber relaxation and PDB templates options. Multiple sequence alignment (MSA) was performed on the sequence database suggested from the GitHub webpage on July 2021 (https://github.com/kalininalab/alphafold_non_docker). Missing residues from PDB sequences were replaced with glycine for AF2 predictions. Predictions generated 5 models, and the highest pLDDT-scoring model was selected.

4.3 | Large-scale prediction of intramolecular isopeptide bonds using Isopeptor, Pfam mapping and creation of new Pfam domains

Isopeptor version v0.0.75 was installed using the pip python package manager and run with default parameters, employing a probability threshold of >0.65 against the AFDB version 4 and the BFVD version 2023 02. AFDB domains detected by Isopeptor were mapped to Pfam version 37 0 entries and assigned to Pfam domains when entries covered at least two of the three residues required for intramolecular isopeptide bond formation. Sortase motifs were annotated within isopeptide bond-containing proteins using the following regex expressions within the last 50 C-terminus amino acids: LP.T[G|A|N|D], NP.TG, LP.GA, LA.TG, NPQTN, IP.TG. Newly created Pfam domains were mapped to AFDB proteins using hmmscan (HMMER version 3.3.2, Eddy, 2011) and filtered considering annotated domain and sequence gathering thresholds. In cases of conflicting annotations, priority was given to domains annotated in Pfam version 37 0. AFDB hits with no corresponding Pfam annotation were used to create new Pfam domain families via sequence clustering, using N-terminal domain boundaries -10/-5 residues from the isopeptide-bonded lysine, and C-terminal domain boundaries +5/+30 residues from isopeptide-bonded asparagine/aspartate for CnaB-like/

CnaA-like domains, respectively. Clustering was performed using MMseqs2 software version 17.b804f (Steinegger & Söding, 2017) via the easy-cluster command and the following flags: cluster-mode 2, covmode 0, min-seq-id 0.25, coverage 0.9, and aligned using MAFFT or Muscle (Edgar, 2004; Katoh & Standley, 2013). The resultant MSAs were used as initial seeds to search the reference proteome database using hmmsearch (HMMER version 3.3.2). Pfam families were built via repeated iterative searches and manual refinement of boundaries, member selection, and inclusion thresholds (which were adjusted for each family to exclude false positives and optimize signal-tonoise).

4.4 | Proximity analysis

For the proximity analysis, we considered amino acid side chains within 6 Å of the centroid formed by the α -carbons of each isopeptide bond triad. β -carbons were excluded from all amino acids except alanine in order to avoid capturing distant side chains that point towards the solvent. The analysis was conducted on the non-redundant set of PDB structures described previously using a custom Python script with Biotite, Biopython, Numpy, and Pandas packages for calculations (see above for versions).

4.5 | Assessing fibrillar adhesin prevalence

For the prediction of fibrillar adhesin prevalence, the FAL_prediction software was downloaded and employed (https://github.com/VivianMonzon/FAL_prediction). FAL_prediction was employed against full-length sequences of Isopeptor-identified AFDB proteins, using a probability threshold of >0.9. The Iupred2a and T-Reks dependencies were downloaded from https://iupred2a.elte.hu/download_new (Mészáros et al., 2018) and https://bioinfo.crbm.cnrs.fr/index.php?route=tools&tool=3 (Jorda & Kajava, 2009), respectively.

4.6 | Detection of disulfide bonds

For the detection of disulfide bonds, disulfide bonds were assigned to cysteine residues with sulfur atoms within an atomic distance lower than the sum of their van der Waals atom radii (i.e., clashing; Bondi, 1964). The analysis was conducted on structures of putative intramolecular isopeptide bond-containing proteins obtained from the AFDB by Isopeptor using a custom python script with the biopython and Pandas packages for calculations (see above for versions).

4.7 | CLIPPER expression

A synthetic gene encoding residues 708–828 of Actinetobacter silvestris ANC4999 fibrillar adhesin B9T28_05395 A0A1Y3CHT7, (Uniprot accession "CLIPPERWT") and a mutant lacking the isopeptideforming lysine residue ("CLIPPERK715A") were ordered from Thermo Fisher Scientific (Table S6), codonoptimized for E. coli. Synthetic genes were inserted into HindIII/KpnI-linearized pOPINF expression vector following polymerase chain reaction with appropriate primers, using the In-FusionTM kit (Takara Bio), following the instructions of Berrow et al., 2007 and verified via DNA sequencing (Eurofins Genomics). The encoded constructs contain an N-terminal hexahistidine tag with a 3C cleavage site, and were transformed into BL21(DE3) Escherichia coli (Thermo Fisher Scientific) using heat-shock, grown in 1 L cultures of Luria Broth supplemented with carbenicillin 100 μg mL⁻¹ until an optical density of 0.8, and induced via addition of isopropyl β-D-1-thiogalactopyranoside to a concentration of 1 mM. Cultures were incubated for 16 h at 18°C (180 RPM), harvested by centrifugation $(4500 \times g, 30 \text{ min})$, the pellets flash-frozen in liquid nitrogen, and stored at -80°C.

4.8 | CLIPPER purification

Pellets were resuspended in phosphate-buffered saline (PBS, 137 mM NaCl, 3 mM KCl, 10 mM Na₂HPO₄, 1.8 mM KH₂PO₄, pH 7.4), lysed using a 120 sonic dismembrator (Fisher Scientific, amplitude 70%, 20 s on, 20 s off, 10 min), and centrifuged (39,000 \times g, 30 min). Supernatant was applied to a 5 mL HisTrap Nickel-NTA column (Cytiva) equilibrated with PBS + 20 mM Imidazole, pH 7.4. A concentration gradient of 20 mM to 500 mM imidazole in PBS was applied over 60 mL for 1 h. Fractions were collected, concentrated, and subjected to size exclusion chromatography (SEC) purification using an EnRich SEC 650 10 × 300 column (BIORAD) equilibrated with PBS for circular dichroism and proteolysis assays or Tris-buffered saline (TBS, 20 mM Tris, 100 mM NaCl, pH 8.0) for crystallization studies. SEC fractions were subjected to SDS-PAGE analysis, mixing 10 μL with 10 μL of 2× Laemli buffer (BioRad), heated at 95°C for 5 min, applied to Novex Tris-Glycine precast SDS-PAGE gels (Thermo), and subjected to 200 V for 30 min in an X-Cell SureLock system (Thermo), and visualized using Instant Blue stain (Fisher Scientific).

4.9 | CLIPPER crystallization and data collection

His-tags of CLIPPER_{WT}/CLIPPER_{K517A} were cleaved using HRV3C protease (Takara Bio), removed via

application to a HisTrap column, and repurified using Sitting-drop vapor-diffusion SEC. sparse of CLIPPERWT/CLIPPERK517A screens 10 mg mL⁻¹ were set up using commercial screens (Molecular Dimensions) and produced crystals in both SG1 screen (condition F1) and Structure Screen 1 + 2 (condition A3). Following optimization, well-diffracting crystals were grown in 1:1 droplet ratios of 5 mg mL-CLIPPER_{WT} with 0.2 M ammonium sulfate, 0.2 M sodium/potassium tartrate, 0.1 M sodium acetate, pH 5.5 in 4 μL droplets (CLIPPER_{K715A} yielded no crystals). Crystals were mounted in LithoLoops (molecular dimensions), flash-cooled in liquid nitrogen without cryoprotectant, and diffraction data collected at the i24 beamline of Diamond Light Source, UK. Data were processed using Xia2 and DIALS (Winter, 2010; Winter et al., 2018) and phases calculated using molecular replacement in CCP4i2 with MOLREP (Potterton et al., 2018; Vagin & Teplyakov, 1997) using the CLIP-PER_{WT} AF2 model and iteratively refined via manual model building with REFMAC and COOT (Emsley et al., 2010; Vagin et al., 2004). The model and structure factors for CLIPPERWT have been deposited at the PDB with the code 9IFR.

4.10 | Circular dichroism

A volume of 1 mL aliquots of CLIPPER_{WT}/CLIP-PER_{K517A} polypeptides were dialyzed overnight at 4°C in 5 L of circular dichroism (CD) buffer (10 mM sodium phosphate, 100 mM sodium fluoride, pH 7.4) using SnakeSkin dialysis tubing (10 kDa cutoff, Thermo). CD spectra were recorded for CLIPPERWT and CLIP-PER_{K517A} using a Jasco J-1500 spectrophotometer continuously purged with nitrogen and fitted with a Peltier temperature control unit. Spectra were obtained from sample volumes of 300 µL in a cuvette with a 1 mm path length (Hellma Analytics) with protein concentrations of 0.36 mg mL⁻¹ (CLIPPER_{WT}) and 0.38 mg mL⁻¹ (CLIPPER_{K715A}) after blanking with CD buffer from the dialysis bucket. Spectra were recorded from 5°C to 95°C at 5°C intervals (thermal unfolding) and subsequently 95-5°C (thermal refolding) over a spectral range of 180-280 nm. High-tension threshold (HT) voltage was continuously recorded to ensure HT was <600 V. Spectra were averaged from four repeat scans and smoothed using a Savitsky-Golay smoothing algorithm over a window of 11 data points.

4.11 | Proteolysis assay

Proteinase K from *Tritirachium album* was used for the proteolysis assay (Sigma Aldrich). A volume of 10 μ L of 1 mg mL⁻¹ CLIPPER_{WT}/CLIPPER_{K517A} was mixed with 10 μ L of 1 mg mL⁻¹ Proteinase K in PBS and aliquoted



into thin-walled PCR tubes (StarLab) on ice. After mixing, aliquots were placed inside a Sensoquest LabCycler (Geneflow) along a heated gradient at 20°C, 30°C, 40°C, or 50°C for 1 h. Aliquots were immediately mixed with SDS running buffer and subjected to SDS-PAGE analysis.

AUTHOR CONTRIBUTIONS

Francesco Costa: Conceptualization; data curation; formal analysis; investigation; methodology; software; validation: visualization: writing - original draft: writing - review and editing. loannis Riziotis: Conceptualization; methodology; software; validation. Antonina Andreeva: Conceptualization; data curation; formal analysis; investigation; methodology; visualization; writing – original draft; writing – review and editing. Delhi Kalwan: Investigation; writing - review and editing. Jennifer de Jong: Investigation; writing - review and editing. Philip Hinchliffe: Formal analysis; validation; writing - review and editing. Fabio Parmeggiani: acquisition: resources: supervision: writing - review and editing. Paul R. Race: Conceptualization; funding acquisition; resources; supervision; writing - review and editing. Steven G. Burston: Conceptualization; methodology; supervision; writing review and editing. Alex Bateman: Conceptualization; funding acquisition; methodology; project administration; writing – original draft; writing – review and editing. Rob Barringer: Conceptualization; data curation; funding acquisition; investigation; methodology; project administration; supervision; visualization; writing original draft; writing - review and editing.

ACKNOWLEDGMENTS

The authors thank Diamond Light Source for beamtime (proposal MX31440) and the staff of beamline i24 for their assistance. The authors also thank Angela Nobbs for discussions regarding fibrillar adhesins and mechanisms of colonization, Alexandr Nemec for discussions regarding the genetic diversity of *Acinetobacter*, and Uli Schwarz-Linek for discussions regarding intramolecular isopeptide bond formation and associated properties. The authors also thank Thom Sharp for hosting Rob Barringer during the period of this work, and Ross Anderson for allowing the use of a Jasco J-1500 spectrophotometer for circular dichroism studies.

FUNDING INFORMATION

This work was supported by the UKRI Biotechnology and Biological Sciences Research Council (BB/X012492/1, BB/W013959/1, BB/T008741/1, and BB/T001968/1), EMBL core funds, and a UKRI Engineering and Physical Sciences Research Council Impact Accelerator Award (EP/X525674/1).

CONFLICT OF INTEREST STATEMENT

The authors declare no conflicts of interest.

DATA AVAILABILITY STATEMENT

The data that support the findings of this study are openly available in Zenodo at http://doi.org/10. 5281/zenodo.15024938. The code used for the analysis is available at: https://github.com/FranceCosta/isopeptide_bonds_global_survey.

ORCID

Rob Barringer https://orcid.org/0000-0002-0948-3761

REFERENCES

- Alegre-Cebollada J, Badilla CL, Fernandez JM. Isopeptide bonds block the mechanical extension of pili in pathogenic *Streptococcus pyogenes*. J Biol Chem. 2010;285;11235–42.
- Alonso-Caballero A, Echelman DJ, Tapia-Rojo R, Haldar S, Eckels EC, Fernandez JM. Protein folding modulates the chemical reactivity of a gram-positive adhesin. Nat Chem. 2020;13: 172–81.
- Barringer R, Parnell AE, Lafita A, Monzon V, Back CR, Madej M, et al. Domain shuffling of a highly mutable ligand-binding fold drives adhesin generation across the bacterial kingdom. Proteins. 2023;91:1007–20.
- Berrow NS, Alderton D, Sainsbury S, Nettleship J, Assenberg R, Rahman N, et al. A versatile ligation-independent cloning method suitable for high-throughput expression screening applications. Nucleic Acids Res. 2007;35:e45.
- Bondi A. van der Waals volumes and radii. J Phys Chem. 1964;68(3): 441–51. https://doi.org/10.1021/j100785a001
- Busscher HJ, van der Mei HC. Microbial adhesion in flow displacement systems. Clin Microbiol Rev. 2006;19:127–41.
- Chaurasia P, Pratap S, von Ossowski I, Palva A, Krishnan V. New insights about pilus formation in gut-adapted *Lactobacillus rhamnosus* GG from the crystal structure of the SpaA backbone-pilin subunit. Sci Rep. 2016;6:28664.
- Cock PJA, Antao T, Chang JT, Chapman BA, Cox CJ, Dalke A, et al. Biopython: freely available Python tools for computational molecular biology and bioinformatics. Bioinformatics. 2009;25: 1422–3
- Costa F, Barringer R, Riziotis I, Andreeva A, Bateman A. Isopeptor: a tool for detecting intramolecular isopeptide bonds in protein structures. Bioinform Adv. 2025;5:vbaf049.
- Doloman A, Besteman MS, Sanders MG, Sousa DZ. Methanogenic partner influences cell aggregation and signalling of *Syntrophobacterium fumaroxidans*. Appl Microbiol Biotechnol. 2024;108:127.
- Echelman DJ, Alegre-Cebollada J, Badilla CL, Chang C, Ton-That H, Fernández JM. CnaA domains in bacterial pili are efficient dissipaters of large mechanical shocks. Proc Natl Acad Sci U S A. 2016;113:2490–5.
- Eddy SR. Accelerated profile HMM searches. PLoS Comput Biol. 2011;7:e1002195.
- Edgar RC. MUSCLE: multiple sequence alignment with high accuracy and high throughput. Nucleic Acids Res. 2004;32:1792–7.
- El Mortaji L, Contreras-Martel C, Moschioni M, Ferlenghi I, Manzano C, Vernet T, et al. The full-length *Streptococcus pneumoniae* major pilin RrgB crystallizes in a fibre-like structure, which presents the D1 isopeptide bond and provides details on the mechanism of pilus polymerization. Biochem J. 2012;441:833–43.
- Emsley P, Lohkamp B, Scott W, Cowtan K. Features and development of Coot. Acta Crystallogr Sect D Biol Crystallogr. 2010;66: 486–501.
- Haft DH, Payne SH, Selengut JD. Archaeosortases and exosortases are widely distributed systems linking membrane transit with posttranslational modification. J Bacteriol. 2012;194:36–48.
- Hagan R, Björnsson R, McMahon S, Schomburg B, Braithwaite V, Bühl M, et al. NMR spectroscopic and theoretical analysis of a

- spontaneously formed lys-asp isopeptide bond. Angew Chem Int Ed. 2010;49:8421–5.
- Harris CR, Millman KJ, van der Walt SJ, Gommers R, Virtanen P, Cournapeau D, et al. Array programming with NumPy. Nature. 2020;585:357–62.
- Heidler TV, Ernits K, Ziolkowska A, Claesson R, Persson K. Porphyromonas gingivalis fimbrial protein Mfa5 contains a von Willebrand factor domain and an intramolecular isopeptide. Commun Biol. 2021;4:106.
- Helgstrand C, Wikoff WR, Duda RL, Hendrix RW, Johnson JE, Liljas L. The refined structure of a protein catenane: the HK97 bacteriophage capsid at 3.44 Å resolution. J Mol Biol. 2003;334: 885–99.
- Hendrickx AA, Budzik JM, Oh S, Schneewind O. Architects at the bacterial surface—sortases and the assembly of pilli with isopeptide bonds. Nat Rev Microbiol. 2011;9:166–76.
- Hendrickx APA, Poor CB, Jureller JE, Budzik JM, He C, Schneewind O. Isopeptide bonds of the major pilin protein BcpA influence pilus structure and bundle formation on the surface of *Bacillus cereus*. Mol Microbiol. 2012;85:152–63.
- Hershko A, Ciechanover A. The ubiquitin system. Annu Rev Biochem. 1998;67:425–79.
- Hu X, Hu H, Melvin J, Clancy K, McCafferty D, Yang W. Autocatalytic intramolecular isopeptide bond formation in gram-positive bacterial pili: a QM/MM simulation. J Am Chem Soc. 2011;133: 478–85.
- Hunter JD. Matplotlib: a 2D graphics environment. Comput Sci Eng. 2007:9:90–5.
- Izoré T, Contreras-Martel C, El Mortaji L, Manzano C, Terrasse R, Vernet T, et al. Structural basis of host cell recognition by the pilus adhesin from *Streptococcus pneumoniae*. Structure. 2010; 18:106–15.
- Jorda J, Kajava AV. T-REKS: identification of Tandem REpeats in sequences with a K-meanS based algorithm. Bioinformatics. 2009;25:2632–8.
- Jumper J, Evans R, Pritzel A, Green T, Figurnov M, Ronneberger O, et al. Highly accurate protein structure prediction with AlphaFold. Nature. 2021;596:583–9.
- Kang H, Coulibaly F, Clow F, Proft T, Baker E. Stabilizing isopeptide bonds revealed in gram-positive bacterial pilus structure. Science. 2007;318:1625–8.
- Kang HJ, Baker EN. Intramolecular isopeptide bonds give thermodynamic and proteolytic stability to the major pilin protein of Streptococcus pyogenes. J Biol Chem. 2009;284:20729–37.
- Kang HJ, Baker EN. Intramolecular isopeptide bonds: protein cross-links built for stress? Trends Biochem Sci. 2011;36:227–35.
- Kang HJ, Baker EN. Structure and assembly of gram-positive bacterial pili: unique covalent polymers. Curr Opin Struct Biol. 2012; 22:200–7.
- Katoh K, Standley DM. MAFFT multiple sequence alignment software version 7: improvements in performance and usability. Mol Biol Evol. 2013;30:772–80.
- Kim RS, Kim RS, Karin EL, Mirdita M, Chikhi R, Steinegger M. BFVD—a large repository of predicted viral protein structures. Nucleic Acids Res. 2025;53:D340–7.
- Kunzmann P, Hamacher K. Biotite: a unifying open source computational biology framework in Python. BMC Bioinform. 2018; 19:346
- Kwon H, Kwon H, Squire CJ, Young PG, Baker EN. Autocatalytically generated Thr-Gln ester bond cross-links stabilize the repetitive Ig-domain shaft of a bacterial cell surface adhesin. Proc Natl Acad Sci U S A. 2014;111:1367–72.
- Lei H, Ma Q, Li W, Wen J, Ma H, Qin M, et al. An ester bond underlies the mechanical strength of a pathogen surface protein. Nat Commun. 2021;12:5082.
- Lipke PN. Not gently down the stream: flow induces amyloid bonding in environmental and pathological fungal biofilms. Mol Cell Biol. 2025;16:e00203–25.

- Lurie-Weinberger MN, Peeri M, Gophna U. Contribution of lateral gene transfer to the gene repertoire of a gut-adapted methanogen. Genomics. 2012;99:52–8.
- McKinney W. Data structures for statistical computing in Python. Proceedings of the 9th Python in science conference. 2010; 56–61.
- Mészáros B, Erdos G, Dosztányi Z. IUPred2A: context-dependent prediction of protein disorder as a function of redox state and protein binding. Nucleic Acids Res. 2018;46:W329–37.
- Mitchell JBO, Nandi CL, McDonald IK, Thornton JM. Amino/aromatic interactions in proteins: is the evidence stacked against hydrogen bonding? J Mol Biol. 1994;239:315–31.
- Monzon V, Bateman A. Large-scale discovery of microbial fibrillar adhesins and identification of novel members of adhesive domain families. J Bacteriol. 2022;204:1–19.
- Monzon V, Lafita A, Bateman A. Discovery of fibrillar adhesins across bacterial species. BMC Genomics. 2021;22:1–14.
- Muszbek L, Adány R, Mikkola H. Novel aspects of blood coagulation factor XIII. I. Structure, distribution, activation, and function. Crit Rev Clin Lab Sci. 1996;33:357–421.
- Nemec A, Radolfová-Křižová L, Maixnerová M, Shestivska V, Španělová P, Higgins PG. Acinetobacter silvestris sp. nov. discovered in forest ecosystems in Czechia. Int J Syst Evol Microbiol. 2022;72:005383.
- Podgorski JM, Freeman K, Gosselin S, Huet A, Conway JF, Bird M, et al. A structural dendrogram of the actinobacteriophage major capsid proteins provides important structural insights into the evolution of capsid stability. Structure. 2023;31:282–94.e5.
- Pointon JA, Smith WD, Saalbach G, Crow A, Kehoe MA, Banfield MA. A highly unusual thioester bond in a pilus adhesin is required for efficient host cell interaction. J Biol Chem. 2010; 285:33858–66.
- Potterton L, Agirre J, Ballard C, Cowtan K, Dodson E, Evans PR, et al. CCP4i2: the new graphical user interface to the CCP 4 program suite. Acta Crystallogr D Struct Biol. 2018;74: 68–84.
- Remaut H, Sleutel M, Sogues A. Auto-crosslinking sporesilk fibers promote endospore and Cry toxin clustering. 2025 [cited 2025 Aug 11]. https://doi.org/10.21203/rs.3.rs-6239967/v1
- Rivas-Pardo JA, Badilla CL, Tapia-Rojo R, Fernández JM. Molecular strategy for blocking isopeptide bond formation in nascent pilin proteins. Proc Natl Acad Sci U S A. 2018;115:9222–7.
- Rost B, Sander C. Conservation and prediction of solvent accessibility in protein families. Proteins. 1994;20:216–26.
- Schwarz-Linek U, Banfield MJ. Yet more intramolecular cross-links in Gram-positive surface proteins. Proc Natl Acad Sci U S A. 2014; 111:1229–30.
- Singh J, Thornton JM. SIRIUS. An automated method for the analysis of the preferred packing arrangements between protein groups. J Mol Biol. 1990;211:595–615.
- Spraggon G, Koesema E, Scarselli M, Malito E, Biagini M, Norais N, et al. Supramolecular organization of the repetitive backbone unit of the *Streptococcus pneumoniae* pilus. PLoS One. 2010;5:e10919.
- Srisantitham S, Walker AL, Markel U, Tezcan AF. De novo design of proteins for autocatalytic isopeptide bond formation. J Am Chem Soc. 2025;147:12338–46.
- Steinegger M, Söding J. MMseqs2 enables sensitive protein sequence searching for the analysis of massive data sets. Nat Biotechnol. 2017:35:1026–8.
- Sumikawa K, Kosaka T, Mayahara N, Matsutani M, Udo K, Yamada M. An aggregation-defective mutant of methanothermobacter sp. CaT2 reveals unique protein-dependent aggregation. Microbes Environ. 2019;34:244–51.
- Tso D, Peebles CL, Maurer JB, Duda RL, Hendrix RW. On the catalytic mechanism of bacteriophage HK97 capsid crosslinking. Virology. 2017;506:84–91.
- Vagin A, Teplyakov A. MOLREP: an automated program for molecular replacement. J Appl Cryst. 1997;30:1022–5.

- Vagin AA, Steiner RA, Lebedev AA, Potterton L, McNicholas S, Long F, et al. REFMAC5 dictionary: organization of prior chemical knowledge and guidelines for its use. Acta Crystallogr D Biol Crystallogr. 2004;60:2184–95.
- Vance TDR, Ye Q, Conroy B, Davies PL. Essential role of calcium in extending RTX adhesins to their target. J Struct Biol X. 2020;4: 100036.
- Varadi M, Bertoni D, Magana P, Paramval U, Pidruchna I, Radhakrishnan M, et al. AlphaFold protein structure database in 2024: providing structure coverage for over 214 million protein sequences. Nucleic Acids Res. 2024;52: D368–75.
- Walden M, Edwards JM, Dziewulska AM, Bergmann R, Saalbach G, Kan S, et al. An internal thioester in a pathogen surface protein mediates covalent host binding. Elife. 2015;4:e06638.
- Waskom M. seaborn: statistical data visualization. J Open Source Softw. 2021;6:3021.
- Winter G. xia2: an expert system for macromolecular crystallography data reduction. J Appl Cryst. 2010;43:186–90.
- Winter G, Waterman D, Parkhurst J, Brewster A, Gildea R, Gerstel M, et al. DIALS: implementation and evaluation of a new integration package. Acta Crystallogr D Struct Biol. 2018;74:85–97.

- Zähner D, Gandhi AR, Stuchlik O, Reed M, Pohl J, Stephens DS. Pilus backbone protein PitB of *Streptococcus pneumoniae* contains stabilizing intramolecular isopeptide bonds. Biochem Biophys Res Commun. 2011;409:526–31.
- Zong Y, Xu Y, Liang X, Keene D, Höök A, Gurusiddappa S, et al. A "collagen hug" model for *Staphylococcus aureus* CNA binding to collagen. EMBO J. 2005;24:4224–36.

SUPPORTING INFORMATION

Additional supporting information can be found online in the Supporting Information section at the end of this article.

How to cite this article: Costa F, Riziotis I, Andreeva A, Kalwan D, de Jong J, Hinchliffe P, et al. A global survey of intramolecular isopeptide bonds. Protein Science. 2025;34(12):e70342. https://doi.org/10.1002/pro.70342